Phonon-drag magnetothermopower oscillations in GaAs/$As_xGa_{1-x}As$ heterojunctions

T. M. Fromhold, P. N. Butcher, G. Qin,* and B. G. Mulimani
Department of Physics, University of Warwick, Coventry CV4 7AL, United Kingdom

J. P. Oxley and B. L. Gallagher
Department of Physics, University of Nottingham, Nottingham, NG7 2RD, United Kingdom
(Received 8 February 1993)

The tensor $\overleftrightarrow{M}$ which determines the heat flux $\mathbf{U}=\overleftrightarrow{M}\mathbf{E}$ in a weak electric field $\mathbf{E}$ is calculated for a two-dimensional electron gas in a perpendicular magnetic field B. The dominant phonon-drag contribution is calculated using Boltzmann transport, allowing for the two-dimensional (2D) character of the electron gas. The Landau levels are taken to have Gaussian line shapes with the rms level width $\gamma=CB^{1/2}$ where C is the only adjustable parameter. Setting $C=0.5$ meV $T^{-1/2}$ gives good agreement with new experimental values of M_{yx} obtained for GaAs/$Al_xGa_{1-x}As$ heterojunctions when B varies between 2 and 10 T and the temperature varies between 1 and 5 K. M_{yx} is negative and contains strong magneto-oscillations in phase with the density of states at the Fermi level. The model also predicts $M_{xx}=0$, whereas experiment gives peak values of $|M_{xx}|$ up to 60% of those of $|M_{yx}|$. We demonstrate that setting $M_{xx}=0$ in the calculation has little effect on the predicted thermopower component S_{xx} but yields poor approximations to the experimental values of S_{yx}.

I. INTRODUCTION

The phonon-drag contribution to magnetothermopower dominates the response of the 2DEG in GaAs/$Al_xGa_{1-x}As$ heterojunctions in the temperature range 1–10 K.[1–3] It has been measured in quantizing magnetic fields by several authors.[4–6] Kubakaddi, Butcher, and Mulimani[2] make calculations in the quantum limit. Quantum oscillations at lower magnetic fields are discussed by Lyo,[3] and Oxley *et al.*[7] use a similar approach to interpret data for a Si metal-oxide-semiconductor field-effect-transistor (MOSFET).

The calculations made in Refs. 2, 3, and 7 all proceed by modifying the Boltzmann theory of phonon drag in three dimensions (3D) (Refs. 8 and 9) to allow for the 2D character of the electron gas. The Boltzmann theory is developed by calculating the tensor $\overleftrightarrow{M}$ which determines the phonon heat flux $\mathbf{U}=\overleftrightarrow{M}\mathbf{E}$ in a weak electric field $\mathbf{E}$. Macroscopic transport equations are used to express the thermopower tensor $\overleftrightarrow{S}$ in terms of $\overleftrightarrow{M}$ and the resistivity tensor $\overleftrightarrow{\rho}$. In these papers attention is focused on the observed behavior of S_{xx} which is reasonably well described by the theory. In the present paper we reverse this approach. Theoretical values of M_{yx} are compared directly with values derived from experimental data for $\overleftrightarrow{S}$ and $\overleftrightarrow{\rho}$. We find that the theory gives a reasonable account of the observed behavior of M_{yx}. However, we also point out that the theory predicts $M_{xx}=0$, in complete contradiction to experiment.

The macroscopic equations relating $\overleftrightarrow{M}$, $\overleftrightarrow{S}$ and $\overleftrightarrow{\rho}$ are given in Sec. II. A detailed transport theory for a magnetoquantized two-dimensional electron gas (2DEG) coupled to 3D phonons is given in Sec. III. Previous accounts[2,3,7] are all very brief and concentrate on S_{xx} so that they do not reveal the major problem concerning M_{xx}. Experimental details are given in Sec. IV. Comparison with new data for $\overleftrightarrow{M}$ and $\overleftrightarrow{S}$ in GaAs/AlGaAs heterojunctions is made in Sec. V, and a possible solution of the M_{xx} problem is discussed in Sec. VI. Technical details relating to the calculations are given in the Appendixes.

II. MACROSCOPIC FORMALISM

We consider a 2DEG moving in the xy plane with a scalar effective mass m^*. We suppose that it is subjected to a magnetic induction field $\mathbf{B}=(0,0,B)$ and is coupled to 3D phonons. The entire system is assumed to be isotropic in the xy plane. We are primarily concerned with two 2D transport tensors: the resistivity tensor $\overleftrightarrow{\rho}$ and the tensor $\overleftrightarrow{M}$ which determines the heat flux $\mathbf{U}=\overleftrightarrow{M}\mathbf{E}$ in an electric field $\mathbf{E}$. The xy isotropy under proper rotations ensures that $\overleftrightarrow{\rho}$ has the properties $\rho_{yy}=\rho_{xx}$ and $\rho_{xy}=-\rho_{yx}$. We work with ρ_{xx} and ρ_{yx}. Onsager symmetry[10] gives $\overleftrightarrow{\rho}(-\mathbf{B})=\tilde{\overleftrightarrow{\rho}}(\mathbf{B})$ so that ρ_{xx} and ρ_{yx} are respectively even and odd functions of B. We show in Appendix A that $\overleftrightarrow{M}$ has the same symmetry properties as $\overleftrightarrow{\rho}$.

In the experimental studies which we discuss, the tensors measured are $\overleftrightarrow{\rho}(\mathbf{B})$ and the thermopower tensor $\overleftrightarrow{S}(\mathbf{B})$. Onsager symmetry gives $\overleftrightarrow{S}(\mathbf{B})=\tilde{\overleftrightarrow{\Pi}}(-\mathbf{B})T^{-1}$ at temperature T where $\overleftrightarrow{\Pi}(\mathbf{B})$ is the Peltier coefficient. This coefficient determines the heat flux $U=\overleftrightarrow{\Pi}(B)J$ produced by an electrical current density J. Since $E=\overleftrightarrow{\rho}(B)J$, we see that $\overleftrightarrow{\Pi}(\mathbf{B})=\overleftrightarrow{M}(\mathbf{B})\overleftrightarrow{\rho}(\mathbf{B})$. The above Onsager symmetry relation therefore reduces to $T\overleftrightarrow{S}(B)=\tilde{\overleftrightarrow{\rho}}(-\mathbf{B})\tilde{\overleftrightarrow{M}}(-\mathbf{B})=\overleftrightarrow{\rho}(\mathbf{B})\tilde{\overleftrightarrow{M}}(\mathbf{B})$. Making further use of the symmetry properties of $\overleftrightarrow{\rho}$ and $\overleftrightarrow{M}$ gives the equations

$$TS_{xx}=\rho_{xx}M_{xx}-\rho_{yx}M_{yx}\ , \tag{1a}$$

$$TS_{yx}=\rho_{yx}M_{xx}+\rho_{xx}M_{yx}\ , \tag{1b}$$

 ©1993 The American Physical Society

where all the tensor elements are understood to be evaluated for $\mathbf{B}=(0,0,B)$. We make extensive use of Eqs. (1) and their solutions for M_{xx} and M_{yx} in terms of S_{xx} and S_{yx} in Sec. V.

III. MICROSCOPIC FORMALISM

To calculate M_{xx} and M_{yx}, we consider only the dominant phonon-drag contribution to the thermoelectric response of the system, and modify the standard Boltzmann theory of magnetotransport in 3D (Refs. 8 and 9) to allow for the 2D character of the electron gas. We confine our attention to the linear transport regime at liquid-helium temperatures. Then it is necessary to consider only acoustic phonons which interact weakly with the heterojunction and consequently retain their 3D character. Thermopower calculations made on this basis when $B=0$ are in good agreement with experimental data.[11,12] We therefore use the same approximation here. We note, however, that in the nonlinear regime optic phonons are generated, and they are affected significantly by the heterojunction.[13–15]

It is convenient to label the acoustic phonons by Roman letters: $a,b,\ldots$, etc. The 2D phonon heat flux in a cube of side L is then

$$\mathbf{U}=L^{-2}\sum_a N_a\hbar\omega_a\boldsymbol{\nu}_a \ , \tag{2}$$

where N_a, ω_a and $\boldsymbol{\nu}_a$ denote the distribution function, frequency, and group velocity of phonon a. Phonons with the thermal equilibrium distribution function

$$N_a^0=[\exp(\hbar\omega_a/k_BT)-1]^{-1} \tag{3}$$

make no contribution to $\mathbf{U}$. We may therefore replace N_a in Eq. (2) by the perturbation N_a^1 produced by the electric field. To determine N_a^1, we use Boltzmann's equation for a homogeneous, steady-state phonon distribution:

$$(\partial N_a/\partial t)_{\rm coll}=-N_a^1/\tau_a+(\partial N_a/\partial t)_{\rm ep}=0 \ . \tag{4}$$

The left-hand side of this equation is the total rate of change of N_a due to all phonon-scattering processes. In the central section we have broken this up into a term $-N_a^1/\tau_a$ which does not involve electrons and a term $(\partial N_a/\partial t)_{\rm ep}$ which does. Their sum must vanish in the steady state. The relaxation time τ_a is given by $\tau_a=\lambda_p/v_a$ where λ_p is a measured phonon mean free path.

We may write Eq. (4) in a form which is convenient for iteration:

$$N_a^1=\tau_a(\partial N_a/\partial t)_{\rm ep} \ . \tag{5}$$

Phonon scattering by electrons is weak. In zeroth order we neglect it altogether and $N_a^1=0$. In first order, we set $N_a^1=0$ on the right-hand side of Eq. (5) to obtain

$$N_a^1=2\tau_a\sum_\alpha\sum_\beta[P_{\alpha\beta}^{\rm em}(a)f_\alpha(1-f_\beta)-P_{\beta\alpha}^{\rm ab}(a)f_\beta(1-f_\alpha)] \ , \tag{6}$$

where we use the following notation. The Greek letters $\alpha,\beta,\ldots$, etc. label electron states in the magnetic *and electric* fields and f_α is the occupation probability of state α. The quantities $P_{\alpha\beta}^{\rm em}(a)$ and $P_{\beta\alpha}^{\rm ab}(a)$ are the transition rates for an electron in a full state $\alpha(\beta)$ to an empty state $\beta(\alpha)$ involving the emission (absorption) of phonon a. The factor of 2 accounts for spin degeneracy (we ignore spin splitting throughout the analysis). The transition rates are calculated in thermal equilibrium. Consequently $P_{\alpha\beta}^{\rm em}(a)$ and $P_{\beta\alpha}^{\rm ab}(a)$ are proportional to N_a^0+1 and N_a^0, respectively.

To linearize N_a^1 in terms of the electric field, we write $f_a=f_a^0+f_\alpha^1$, where

$$f_\alpha^0\equiv f^0(\epsilon_\alpha)=[\exp\{(\epsilon_\alpha-\epsilon_F)/k_BT\}+1]^{-1} \tag{7}$$

is the Fermi-Dirac function and f_α^1 is linear in E and remains to be calculated. In Eq. (7), ϵ_α is the energy of state α in the magnetic and electric fields, ϵ_F is the Fermi level, and T is the temperature. When f_α^1 is neglected, Eq. (6) yields $N_a^1=0$ because of detailed balance. When f_α^1 is retained to first order we find, after some manipulation of detailed balance relations,[1] that

$$N_a^1=-\frac{2\tau_a}{k_BT}\sum_\alpha\sum_\beta\Gamma_{\alpha\beta}(\alpha)\left[\frac{f_\alpha^1}{df_\alpha^0/d\epsilon_\alpha}-\frac{f_\beta^1}{df_\beta^0/d\epsilon_\beta}\right] \ , \tag{8}$$

where

$$\Gamma_{\alpha\beta}(a)=P_{\alpha\beta}^{\rm em}(a)f_\alpha^0[1-f_\beta^0] \tag{9a}$$

$$=P_{\beta\alpha}^{\rm ab}(a)f_\beta^0[1-f_\alpha^0] \ . \tag{9b}$$

Inspection of this equation shows that $\Gamma_{\alpha\beta}(a)$ may be identified with the thermal equilibrium electron flux either from α to β due to phonon emission or from β to α due to phonon absorption. The two interpretations are identical because of detailed balance.

To calculate f_α^1, we follow Refs. 2, 3, 8, and 9 and suppose that $\mathbf{E}$ is established adiabatically. Before $\mathbf{E}$ is applied, the energy of the magnetoquantized state α has a zero-field value which we denote by ϵ_α^0. The occupation probability of state α is then given by Eq. (7) as $f^0(\epsilon_\alpha^0)$. By hypothesis, it does not change when a field $\mathbf{E}=(E,O,O)$ is switched on. Hence $f_\alpha=f^0(\epsilon_\alpha^0)$ in the presence of the field. However, the energy of state α *does* change from ϵ_α^0 to $\epsilon_\alpha^0+eEx_\alpha$, where x_α is determined in Appendix B. Consequently,

$$\begin{aligned}f_\alpha^1&=f_\alpha-f_\alpha^0\\&=f^0(\epsilon_\alpha^0)-f^0(\epsilon_\alpha)\\&\simeq-[df^0(\epsilon_\alpha)/d\epsilon_\alpha]eEx_\alpha \ .\end{aligned} \tag{10}$$

When this result is substituted into Eq. (8), we must set $E=0$ in all the energies involved to achieve a consistent linearization. Leaving this understood, we find that Eq. (2) reduces to $\mathbf{U}=\overleftrightarrow{M}\mathbf{E}$, with

$$M_{xx}=\sum_a\sum_\alpha\sum_\beta(2\tau_\alpha e\hbar\omega_a/k_BTL^2)\Gamma_{\alpha\beta}(a)(x_\alpha-x_\beta)v_{ax} \tag{11a}$$

and

$$M_{yx}=\sum_a\sum_\alpha\sum_\beta(\tau_\alpha 2e/k_BTL^2)\Gamma_{\alpha\beta}(a)v_{ay}(x_\alpha-x_\beta)\ . \quad (11b)$$

Equation (11) summarizes our final formulas in the general case. It only remains to fill in the details relevant to GaAs/$Al_xGa_{1-x}As$ heterojunctions which are given in Appendix B. Thus $a=(\mathbf{q},s)$, where $\mathbf{q}$ is a 3D phonon wave vector and, in the usual approximation, s labels two degenerate transverse acoustic modes and one longitudinal acoustic mode. Moreover, in the Landau gauge for the magnetic potential $\mathbf{A}=(0,Bx,0)$, crystal momentum is conserved in the y direction which leads to Eq. (B5): $x_\alpha-x_\beta=-l^2q_y$,

$$M_{xx}=-(l^2 2e/k_BTL^2)\sum_q\sum_s\tau_{\mathbf{q}s}\hbar\omega_{\mathbf{q}s}v_s(q_xq_y/q)\Gamma(\mathbf{q}s)\ , \quad (12a)$$

$$M_{yx}=-(l^2 2e/k_BTL^2)\sum_q\sum_x\tau_{\mathbf{q}s}\hbar\omega_{\mathbf{q}s}v_s(q_y^2/q)\Gamma(\mathbf{q}s)\ , \quad (12b)$$

where

$$\Gamma(\mathbf{q}s)=\sum_\alpha\sum_\beta\Gamma_{\alpha\beta}(\mathbf{q}s)\ . \quad (12c)$$

The xy isotropy of the system guarantees that $\Gamma(\mathbf{q},s)$ is independent of the orientation of $\mathbf{q}_\parallel=(q_x,q_y)$. Consequently Eq. (12a) gives $M_{xx}=0$. In Sec. V, we emphasize that this result is in complete contradiction to experiment, while Eq. (12b) gives a reasonable account of the observed behavior of M_{yx}.

We see immediately that M_{yx} is negative. To evaluate it we follow Appendix B by putting $\alpha=nk_y$ and $\beta=n'k_y'$, where n and n' are Landau level indices and k_y and k_y' are wave numbers. Because crystal momentum is conserved in the y direction, we find from Eqs. (12c), (9b), and (B9) that

$$\Gamma(\mathbf{q}s)=\sum_n\sum_{n'}\sum_{k_y}\Gamma_{nk_y,n'k_y-q_y}(\mathbf{q}s)\ , \quad (13)$$

in which

$$\Gamma_{nk_y n'k_y-q_y}=C_{nn'}(\mathbf{q}s)N_{qs}^0 f^0_{n'k_y-q_y}[1-f^0_{nk_y}]\times\delta[\epsilon_{nk_y}-\epsilon_{n'k_y-q_y}-\hbar\omega_{\mathbf{q}s}]\ , \quad (14)$$

where the factor $C_{nn'}(\mathbf{q}s)$ involves matrix elements of the electron-phonon interaction as described in Appendix B.

We see by inspection that k_y only appears in Eq. (14) through the energies ϵ_{nk_y} and $\epsilon_{n'k_y-q_y}$, which are randomized by Landau-level broadening. We therefore take a simple system average by integrating Eq. (14) over $\epsilon=\epsilon_{nk_y}$ and $\epsilon'=\epsilon_{n'k_y-q_y}$ with a weighting factor $p(\epsilon-\epsilon_n)p(\epsilon'-\epsilon_{n'})$, where $\epsilon_n=(n+\frac{1}{2})\hbar\omega_c$ is the energy of the nth Landau level in the absence of disorder, and

$$p(x)=(\gamma\sqrt{2\pi})^{-1}\exp(-x^2/2\gamma^2) \quad (15)$$

is a convenient normalized line-shape function with linewidth γ. Then we find that

$$\Gamma(\mathbf{q}s)=N_{qs}^0(L^2/2\pi l^2)\sum_n\sum_{n'}C_{nn'}(\mathbf{q}s)I_{nn'}(\hbar\omega_{\mathbf{q}s})\ , \quad (16a)$$

where the second factor is the degeneracy of the nth Landau level and

$$I_{nn'}(\hbar\omega_{\mathbf{q}s})=\int d\epsilon\, p(\epsilon-\epsilon_n)p(\epsilon+\hbar\omega_{\mathbf{q}s}-\epsilon_{n'})\times f^0(\epsilon)[1-f^0(\epsilon+\hbar\omega_{\mathbf{q}s})]\ . \quad (16b)$$

Once $\Gamma(\mathbf{q},s)$ is evaluated from Eq. (16), with the help of Eq. (15) we may use Eq. (12b) to complete the calculation of M_{yx}. The theory contains only one parameter: γ. All the other parameters of the heterojunction can be related to measured quantities as described in Appendix C.

IV. EXPERIMENTAL DETAILS

The samples measured in Nottingham are long Hall bars of width 0.25 mm and maximum voltage probe separation 2.6 mm. They were grown by molecular-beam epitaxy (MBE), and at liquid-helium temperatures have a mobility of 43 $m^2v^{-1}s^{-1}$ and an areal electron density $n_s=5.2\times10^{15}$ m^{-2}. The chip on which the device is formed is 0.3 mm thick, 1 mm wide, and 12 mm long.

The samples are attached at their ends by indium faced clamps to copper blocks which contain heaters and calibrated Ge thermometers. One of these is thermally linked to a high stability 1-K pumped He pot and forms the heat sink. The other forms the heat source. The experimental technique used to measure the temperature gradient is described by Gallagher *et al.*[12] We use the resistances at two points across the sample as "thermometers" to measure the temperature gradient. The temperature difference established between the voltage probes is set close to 50 mK at each measuring temperature. The thermoelectric voltages are measured using an EM Electronics N11 nanovoltmeter with an overall accuracy of better than 5%.

V. COMPARISON OF THEORY WITH EXPERIMENT

We discuss first of all new measurements made at the University of Nottingham, on a sample with $n_s=5.2\times10^{15}$ m^{-2}. The quantities ρ_{yx}, ρ_{xx}, S_{yx} and S_{xx} are all measured as functions of B. These values are then used in Eq. (1) to determine M_{yx} and M_{xx}. The results at 1.275 K are given in Fig. 1 for M_{xx} as curve 1 and for M_{yx} as curve 2. We see that, as predicted, M_{yx} is negative. Moreover, $|M_{yx}|$ oscillates in phase with ρ_{xx} with its minima located at the same B values as the Hall plateaus.

Curve 3 in Fig. 1 is the theoretical curve for M_{yx} with $\lambda_p=0.75$ mm (as measured) and $\gamma=CB^{1/2}$ meV with $C=0.5$ meV $T^{-1/2}$. The square-root B dependence has previous theoretical and experimental support.[16–19] Setting $C=0.5$ meV $T^{-1/2}$ gives a reasonable fit to the experimental data. The magnitude of M_{yx} is sensitive to C. Halving C roughly doubles the heights predicted for the maxima of $|M_{yx}|$. The experimental peak at 6 T associated with the $n=1$ Landau level is sharper than predicted because of the effect of spin splitting. For higher Landau

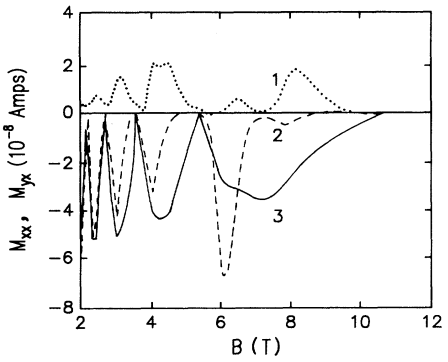

FIG. 1. A comparison of experimental and theoretical values of M_{yx} and M_{xx} for a Nottingham sample with $n_s=5.2\times10^{15}$ m^{-2} at 1.275 K (Ref. 10). Curve 1: experimental values of M_{xx}. Curve 2: experimental values of M_{yx}. Curve 3: theoretical values of M_{yx}. For curve 3, $\gamma=0.5B^{1/2}$ meV and $\lambda_p=0.75$ mm.

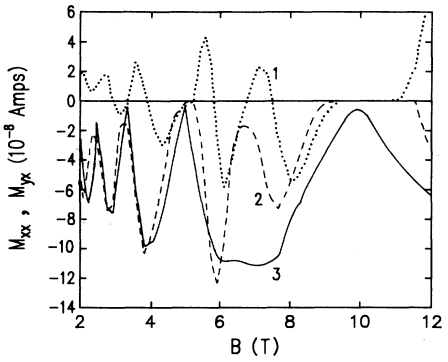

FIG. 3. A comparison of experimental and theoretical values of M_{yx} and M_{xx} for Fletcher's sample 2 (Ref. 5) with $n_s=4.8\times10^{15}$ m^{-2} at 1.8 K. Curve 1: experimental values of M_{xx}. Curve 2: experimental values of M_{yx}. Curve 3: theoretical values of M_{yx}. In curve 3, $\gamma=1$ meV and $\lambda_p=0.63$ mm.

levels spin splitting is unimportant and the small differences between theory and experiment originate from our assumed Gaussian density of states. The predicted shape primarily depends on the density of states within the Landau levels, and is therefore not significantly changed by introducing localized states into the level tails.[3] Curve 1 in Fig. 1 gives the experimental data for M_{xx}. It has peak magnitudes comparable with those of $|M_{yx}|$. We recall that the theoretical prediction is $M_{xx}=0$.

Figure 2 shows similar comparisons of theory and experiment for the same sample at 5.005 K, for which λ_p is found to be 0.41 mm. At this temperature, spin splitting is no longer resolved anywhere in the experimental data. The theoretical curves are calculated in the same way as in Fig. 1 with $C=0.5$ meV $T^{-1/2}$. The behavior is not significantly different from that found at 1.275 K.

We have also made calculations for some of the samples studied experimentally by Fletcher and coworkers.[5,6] We set $\gamma=1$ meV in all cases for comparison with the result of Lyo.[3] Figure 3 is drawn for sample 2 in Ref. 5 at 1.8 K with $n_s=4.8\times10^{15}$ m^{-2} and $\lambda_p=0.63$ mm. Curves 1, 2, and 3 show experimental values of M_{xx}, experimental values of M_{yx}, and theoretical values of M_{yx}, respectively. As before, the $n=1$ Landau peak in $|M_{yx}|$ is spin split experimentally whereas we ignore spin splitting in the theory. This apart, we see that taking $\gamma=1$ meV yields theoretical $|M_{yx}|$ peaks in satisfactory agreement with the experimental data. In contrast to the Nottingham data, however, M_{xx} oscillates about zero. The zeros follow no simple pattern. For sample $BP4$ in Ref. 6 at 4.03 K with $n_s=6.24\times10^{15}$ m^{-2} and $\lambda_p=1.3$ mm,[3,6] we recover the results of Lyo for $-S_{xx}$ from Eq. (1a) by using his approximations $\rho_{xx}=0$ and $\rho_{yx}=-B/n_se$. In determining S_{yx} from Eq. (1b), however, it is essential to use the experimental values of ρ_{xx} because setting $\rho_{xx}=0$ and giving M_{xx} its theoretical value of zero yields $S_{yx}=0$.

Curve 1 of Fig. 4 shows experimental $-S_{xx}$ data for the Nottingham sample at $T=2.937$ K. Curve 2 shows

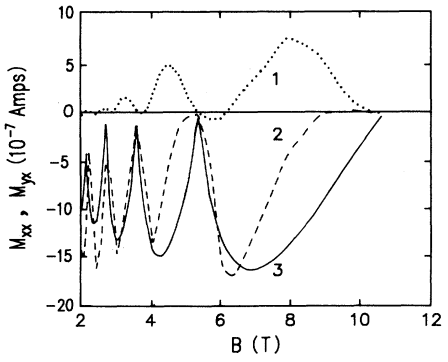

FIG. 2. A comparison of experimental and theoretical values of M_{yx} and M_{xx} for the Nottingham sample with $n_s=5.2\times10^{15}$ m^{-2} at 5.005 K (Ref. 10). Curve 1: experimental values of M_{xx}. Curve 2: experimental values of M_{yx}. Curve 3: theoretical values of M_{yx}. For curve 3, $\gamma=0.5B^{1/2}$ meV and $\lambda_p=0.41$ mm.

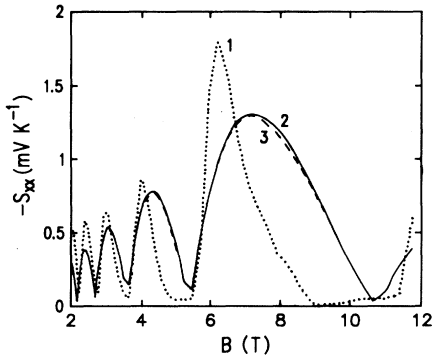

FIG. 4. A comparison of experimental and theoretical values of $-S_{xx}$ for the Nottingham sample with $n_s=5.2\times10^{15}$ m^{-2} at $T=2.937$ K. Curve 1: Experimental values of $-S_{xx}$. Curve 2: theoretical values of $-S_{xx}$ ($M_{xx}=0$). Curve 3: $-S_{xx}$ calculated using empirical M_{xx} data. For curves 2 and 3, $\gamma=0.5B^{1/2}$ meV and $\lambda_p=0.6$ mm.

the corresponding theoretical results calculated from Eq. (1a) using the experimental values of ρ_{xx} and ρ_{yx} and the theoretical values of M_{yx} and M_{xx}. It is in good agreement with the experimental curve 1, which is surprising because we have shown in Fig. 1 that the theory is seriously in error in predicting $M_{xx}=0$. To see why this is so, in curve 3 we show $-S_{xx}$ calculated from Eq. (1a) using the theoretical value of M_{yx} and the *experimental* value of M_{xx}. There is hardly any difference between curves 1 and 2. The reason is that the second term on the right-hand side of Eq. (1a) is overwhelmingly dominant, as emphasized by Fletcher *et al.*[5], and so the value of M_{xx} has little effect on the predicted values of $-S_{xx}$, which are always positive, as observed, with peak heights in fair accord with the experimental data.

The prediction $M_{xx}=0$ is only revealed as a serious deficiency of the model for calculating $\vec{S}$ when the measured and calculated S_{yx} curves are compared. Previous theoretical interpretations of GaAs/(Al_xGa_{1-x})As data have concentrated exclusively on S_{xx} and have consequently overstressed the success of the Boltzmann transport theory because S_{xx} depends so weakly on M_{xx}.[2,3] Curve 1 of Fig. 5 shows experimental S_{yx} data for the Nottingham sample at $T=2.937$ K. Curve 2 is the theoretical result obtained from Eq. (1b) using experimental $\vec{\rho}$ values and the theoretical values of M_{yx} and M_{xx}. It is completely at variance with the data because S_{yx} is very sensitive to M_{xx}. To illustrate this, in curve 3 we show S_{yx} calculated from Eq. (1b) using the theoretical value of M_{yx} and the *experimental* value of M_{xx}. This time, in complete contrast to the behavior of S_{xx}, changing M_{xx} in this way alters the predicted values of S_{yx} so much that curve 3 is in very good agreement with the data. This is because the first term on the right-hand side of Eq. (1b) dominates the behavior of S_{yx} to such an extent that the errors in the theoretical value of M_{yx} of the type shown in Fig. 1 have a negligible effect on the calculated values of S_{yx}.

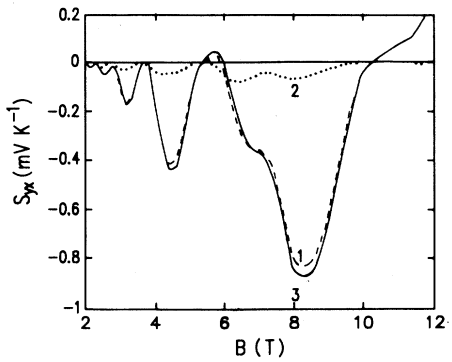

FIG. 5. A comparison of experimental and theoretical values of S_{yx} for the Nottingham sample with $n_s=5.2\times10^{15}$ m^{-2} at $T=2.937$ K. Curve 1: Experimental values of S_{yx}. Curve 2: theoretical values of S_{yx} ($M_{xx}=0$). Curve 3: S_{yx} calculated using empirical M_{xx} data. For curves 2 and 3, $\gamma=0.5B^{1/2}$ meV and $\lambda_p=0.6$ mm.

VI. CONCLUSIONS

The theoretical curves in Figs. 1–5 are all drawn with $\gamma\sim1$–1.5 meV, while the largest value of $k_BT\sim0.5$ meV. Thus in these samples we are always concerned with relatively wide Landau subbands. In this case, the oscillations of $|M_{yx}|$ and $-S_{xx}$ are in phase with those of ρ_{xx}, which are in turn in phase with the oscillations of the density of states at the Fermi level $D(E_F)$. In Ref. 20, we point out that for very narrow Landau subbands with $\gamma<0.06B^{1/2}$ meV, the peaks in $D(E_F)$ greatly enhance screening by the 2DEG which suppresses the electron-phonon interaction. In that case the theory predicts *minima* for $|M_{yx}|$ and $-S_{xx}$ at the corresponding magnetic fields, while the maxima of these quantities occur at field values corresponding to $D(E_F)$ *minima,* for which the screening remains small.

The Landau-level width is determined by parameter C in the relation $\gamma=CB^{1/2}$. To secure good agreement with experimental data here, we need to take $C=0.5$ meV T$^{-1/2}$, which is 8.3 times larger than the value of 0.06 meV T$^{-1/2}$ necessary to produce the 180° phase shift between maxima in $|M_{yx}|$ and $D(E_F)$. With $C=0.5$ meV T$^{-1/2}$, the predicted orders of magnitudes and phases of the $-S_{xx}$ oscillations agree well with experiment, and the temperature dependence is qualitatively correct.

The major discrepancy between the theory and the raw experimental data, which is only revealed when the S_{yx} curves are considered, is the prediction that $M_{xx}=0$. This has its origin in the assumption that the electrons can be adequately described by a diagonal density matrix which does not change when the electric field is switched on. Before this assumption can be removed, a substantial development of electron transport theory in the integer quantum Hall regime is required. The electrons must be described by a full density matrix and the Landau-level broadening must be taken into account self-consistently. Theories on these lines exist in the case when the electron scattering is elastic,[13,17] but they do not give a satisfactory account of the quantized behavior of ρ_{yx}. It is for this reason that we have consistently used *experimental* values of $\vec{\rho}$ in calculating $\vec{S}$ from $\vec{M}$. This difficulty is not so serious in the interpretation of phonon-drag magnetothermopower data as the prediction $M_{xx}=0$. Nevertheless, it is another unsatisfactory feature of the theory. We suggest that it should be looked at before the M_{xx} problem is addressed. A deeper understanding of the calculation of $\vec{\rho}$ in the presence of both elastic and inelastic scattering processes would throw light on the theory of phonon-drag magnetothermopower which is inherently more complicated because it is dominated by inelastic scattering.

ACKNOWLEDGMENT

The authors would like to thank the Science and Engineering Research Council for financial support.

APPENDIX A: THE SYMMETRY PROPERTIES OF $M(B)$

The xy isotropy under proper rotations implies that $\overleftrightarrow{M}(\mathbf{B})$ has the same symmetry as $\overleftrightarrow{\rho}(\mathbf{B})$. Consequently $M_{yy}=M_{xx}$ and $M_{xy}=-M_{yx}$. Here we show that $\overleftrightarrow{M}(-\mathbf{B})=\overleftrightarrow{M}(\mathbf{B})$ when $\mathbf{B}=(0,0,B)$, so that M_{xx} and M_{yx} are respectively even and odd functions of B. Unlike the corresponding identity for $\overleftrightarrow{\rho}$, which is given in Sec. II, this result does not follow from time-reversal symmetry. It is, instead, a consequence of gauge invariance and xy isotropy.

To see this we note that the magnetic induction field appears in the Hamiltonian through the kinetic-energy operators for the individual electrons $K=(\mathbf{p}+e\mathbf{A})^2/2m^*$, where $\mathbf{p}=-i\hbar\nabla$. In Appendix B, we write $A=(0,Bx,0)$ to calculate $\overleftrightarrow{M}(B)$ in a right-handed coordinate system $Oxyz$. Now let us repeat the calculation with a new vector potential $\mathbf{A}_N=(By,0,0)$ which reverses the sign of $\mathbf{B}$. The result is $\overleftrightarrow{M}(-\mathbf{B})$ because the system is gauge invariant. We may, however, put the new Hamiltonian in the same form as the old by introducing new coordinates $x'=y$ and $y'=x$. Then K becomes $(\mathbf{p}'+e\mathbf{A}')^2/2m^*$ with $\mathbf{p}'=-i\hbar\nabla'$ and $\mathbf{A}'=(0,Bx',0)$. When $\overleftrightarrow{M}$ is calculated from this new Hamiltonian in $Ox'y'z$ the result is simply $\overleftrightarrow{M}(\mathbf{B})$ again, which transforms to $\overleftrightarrow{M}(\mathbf{B})$ in $Oxyz$ because $M_{xx}(\mathbf{B})=M_{yy}(\mathbf{B})$. Thus we obtain the desired result $\overleftrightarrow{M}(-\mathbf{B})=\overleftrightarrow{M}(\mathbf{B})$.

APPENDIX B: THEORETICAL DETAILS

At liquid-helium temperatures, only acoustic-phonon modes contribute to phonon drag. We therefore write the phonon label a as $(\mathbf{q},s)$, where $\mathbf{q}$ is the 3D phonon wave vector and s takes three values which label one longitudinal mode ($s=l$) and two degenerate transverse modes ($s=t$) with group velocities $v_l=v_l\mathbf{q}/q$ and $v_t=v_t\mathbf{q}/q$, respectively, where v_l and v_t are the speeds of longitudinal and transverse sound waves.

We suppose that the electrons are entirely confined to the GaAs side of the heterojunction. Only the ground electric subband is occupied. We write its z-dependent wave function in the form

$$\phi(z)=(b^3/2)^{1/2}z\exp(-bz/2)\ , \tag{B1}$$

where b is determined variationally to be[16]

$$b=k_F[33e^2k_F/32\pi\epsilon_0\kappa_s\epsilon_F]^{1/3}\ . \tag{B2}$$

Here, κ_s is the static dielectric constant and k_F and ϵ_F are the Fermi wave number and energy when $B=0$.

We use the vector potential $\mathbf{A}=(0,Bx,0)$ for which the electron state label $\alpha=nk_y$ where $n=0,1,2,\ldots$ labels the Landau levels and $\hbar k_y$ is the eigenvalue of p_y. When $\mathbf{E}=0$, the 2D wave function is[16,21]

$$\psi_{nk_y}=L^{-1/2}e^{ik_yy}X_n(x+l^2k_y)\ , \tag{B3}$$

where X_n denotes the nth harmonic-oscillator wave function and $l=(\hbar/eB)^{1/2}$ is the magnetic length. The corresponding energy is

$$\epsilon_{nk_y}=(n+\tfrac{1}{2})\hbar\omega_c+\delta\epsilon_n(k_y)\ , \tag{B4}$$

where $\omega_c=eB/m^*$ is the cyclotron frequency and $\delta\epsilon_n(k_y)$ is a random energy which takes approximate account of the Landau-level broadening.

When $\mathbf{E}=(E,0,0)$, the scalar potential is eEx. To first order in E the energy of state $\alpha=nk_y$ increases by $eE(-l^2k_y)$. Hence, in Eq. (10), $x_\alpha=-l^2k_y$ and, in Eq. (11) (with $\beta=n'k_y'$), $x_\beta=-l^2k_y'$. Consequently,

$$\begin{aligned}x_\alpha-x_\beta&=-l^2(k_y-k_y')\\&=-l^2q_y\end{aligned} \tag{B5}$$

because, as we show below, $\Gamma_{\alpha\beta}$ conserves crystal momentum in the y direction. The perturbation of ψ_{nk_y} by the electric field is negligible.

The electrons interact with acoustic phonons through both deformation and piezoelectric potentials. The interaction Hamiltonian in either case takes the standard form

$$H_{\rm ep}=\sum_{\mathbf{q}s}[V_{\mathbf{q}s}e^{i\mathbf{q}\cdot\mathbf{r}}a_{\mathbf{q}s}+V_{\mathbf{q}s}^*e^{i\mathbf{q}\cdot\mathbf{r}}a_{\mathbf{q}s}^+]\ , \tag{B6}$$

where $a_{\mathbf{q}s}$ and $\alpha_{\mathbf{q}s}^+$ are phonon annihilation and creation operators. To evaluate $\Gamma_{\alpha\beta}(a)$, we use Eq. (9b) with $\alpha=nk_y$, $\beta=n'k_y'$, and $a=\mathbf{q}s$. Then we have

$$\Gamma_{nk_y,n'k_y'}(qs)=P^{\rm ab}_{n'k_y'nk_y}(qs)f^0_{n'k_y'}[1-f^0_{nk_y}]\ , \tag{B7}$$

where, since phonon absorption is involved,

$$\begin{aligned}P^{\rm ab}_{n'k_y',nk_y}(qs)=&\frac{2\pi}{\hbar}N^0_{\mathbf{q}s}|V_{\mathbf{q}s}|^2\delta[\epsilon_{nk_y}-\epsilon_{n'k_y'}-\hbar\omega_{\mathbf{q}s}]\\&\times|\langle nk_y|e^{i\mathbf{q}\cdot\mathbf{r}}|n'k_y'\rangle|^2\ .\end{aligned} \tag{B8}$$

Inspection shows that the squared magnitude of the electron matrix is the product of the following three factors:[22,23]

$$\left|L^{-1}\int_0^L dy\,\exp[i(k_y'+q_y-k_y)y]\right|^2=\delta_{k_y',k_y-q_y}\ , \tag{B9}$$

$$\begin{aligned}\Delta_z(q_z)&=\left|\int_{-\infty}^{\infty}dz\,\phi(z)^2\exp(iq_zz)\right|^2\\&=[b^2/(b^2+q_z^2)]^3\ ,\end{aligned} \tag{B10}$$

where we have used Eq. (B1) and

$$\begin{aligned}\Delta_{nn'}(q_\parallel)&=\left|\int_{-\infty}^{\infty}dy\,X_n(x+l^2k_y)X_{n'}(x+l^2k_y')e^{iq_xx}\right|^2\\&=(n_s!/n_l!)\chi^{n_l-n_s}e^{-\chi}[L_{n_s}^{n_l-n_s}(\chi)]^2\ .\end{aligned} \tag{B11}$$

In Eq. (B11), $\chi=(q_\parallel l)^2/2$, with $q_\parallel=|q_\parallel|=(q_x^2+q_y^2)^{1/2}$. n_s and n_l are the smallest and largest of n and n', respectively, and $L_n^m(\chi)$ is the associated Laguerre polynomial. In deriving Eq. (B11), use is made of the momentum-conservation condition Eq. (B9) to eliminate k_y'. k_y may also be removed by a uniform translation of the x coordinate. Only the length $q_\parallel$ of $\mathbf{q}_\parallel$ is involved in the final result, which is derived by using formula 7.377 in Ref. 24. The quantity $C_{nn'}(\mathbf{q}s)$ in Eq. (14) is identified by comparing Eq. (14) with Eq. (B7) to Eq. (B11). Thus we find that

$$C_{nn'}(\mathbf{q}s)=\frac{2\pi}{\hbar}\Delta_z(q_z)\Delta_{nn'}(q_\parallel)|V_{qs}|^2 . \quad \text{(B12)}$$

Only the piezoelectric interaction contributes to $|V_{qt}|^2$ for each of the transverse modes, and is given by

$$|V_{qt}|^2=f_t(eh_{14})^2A_t/q^2 , \quad \text{(B13)}$$

where

$$f_t=\hbar\omega_{qt}|2\epsilon(\mathbf{q}_\parallel)^2\rho v_t^2L^3 .$$

Here ρ and h_{14} are respectively the density and piezoelectric coefficient and $A_t=(8q_\parallel^2q_z^4+q_\parallel^6)/4q^6$ is an anisotropy factor.[21] The longitudinal modes scatter off electrons through the deformation-potential interaction as well as the piezoelectric interaction. The effects are additive and we can account for both interactions by writing

$$|V_{ql}|^2=f_l[D^2+(eh_{14})^2A_l/q^2] . \quad \text{(B14)}$$

Here, $f_l=f_t(v_t/v_l)^2$, D is the deformation potential, and $A_l=9q_\parallel^4q_z^2/2q^6$ is another anisotropy factor.[25]

The quantity $\epsilon(q_\parallel)$ which appears in the denominator of $|V_{qs}|^2$ is the dielectric function which takes account of the screening of the bare interactions. It is a scalar depending only on $q_\parallel$ because we use the single subband approximation for an isotropic 2DEG. The function is only weakly dependent on T and we evaluate it for $T=0$ with the density response function set equal to the density of states at the Fermi level $D(B)$, i.e., in the Thomas-Fermi approximation.[14,16] We use the notation $D(B)$ because the density of states at ϵ_F is evaluated as a function of B for each sample from the known electron concentration n_s by using the equations

$$D(B)=(\pi l^2)^{-1}\sum_n p(\epsilon_F-\epsilon_n) \quad \text{(B15a)}$$

and

$$n_s=(\pi l^2)^{-1}\sum_n\int_{-\infty}^{\epsilon_F}p(\epsilon-\epsilon_n)d\epsilon , \quad \text{(B15b)}$$

where $p(x)$ is the normalized line-shape function (15). With these approximations,[22,23]

$$\epsilon(q_\parallel)=1+[e^2D(B)/2\epsilon_0\kappa_sq_\parallel]F(q_\parallel)\Delta_{NN}(q_\parallel) , \quad \text{(B16)}$$

where $F(q_\parallel)$ is the form factor

$$F(q_\parallel)=\int dz\int dz'|\phi(z)|^2|\phi(z')|^2\exp[-q_\parallel|z-z'|] \quad \text{(B17a)}$$

$$=[8+9q_\parallel/b+3(q_\parallel/b)^2]/8[1+q_\parallel/b]^3 \quad \text{(B17b)}$$

which allows for the spread in the z direction of the electric subband wave function $\phi(z)$ given by Eq. (B1). The matrix element $\Delta_{NN}(q_\parallel)$ is given by Eq. (B11), where N is the index of the Landau level closest to the Fermi energy. It allows for the localization by the magnetic field of the electron wave functions in the xy plane. Both $F(q_\parallel)$ and $\Delta_{NN}(q_\parallel)$ are unity when $q_\parallel=0$ and fall off with increasing $q_\parallel$. When these two factors are set equal to unity, Eq. (B16) reduces to the Thomas-Fermi approximation to $\epsilon(q_\parallel)$ for an ideal 2DEG.[16]

APPENDIX C. PARAMETER VALUES

The numerical values of the GaAs parameters used in the calculations are $\kappa_s=12.9$, $m^*=0.067m_0$, $v_l=5140$ ms^{-1}, $V_t=3040$ ms^{-1}, $\rho=5300$ kg m^{-3}, $D=-9.3$ eV, and $h_{14}=1.2\times10^9$ V m^{-1}. Apart from m^*, these are the values used by Lyo,[3] who puts $m^*=0.70m_0$. The phonon relaxation time τ_{qs} is given by λ_p/v_s, where λ_p is a phonon mean free path which is measured for every sample we discuss along with the electron density n_s.

*Present address: Department of Physics, Nanjing University, Nanjing 210008, People's Republic of China.

[1]D. G. Cantrell and P. N. Butcher, J. Phys. C **20**, 1985 (1987); **20**, 1993 (1987).
[2]S. S. Kubakaddi, P. N. Butcher, and B. G. Mulimani, Phys. Rev. B **40**, 1377 (1989).
[3]S. K. Lyo, Phys. Rev. B **40**, 6458 (1989).
[4]M. A. Brummell, T. H. H. Vuong, R. J. Nicholas, J. C. Portal, M. Razeghi, K. Y. Cheng, and A. Y. Cho, Solid State Commun. **57**, 377 (1986).
[5]R. Fletcher, J. C. Maan, K. Ploog, and G. Weimann, Phys. Rev. B **33**, 7122 (1986).
[6]R. Fletcher, M. D'Iorio, W. T. Moore, and R. Stoner, J. Phys. C **21**, 2681 (1988).
[7]J. P. Oxley, B. L. Gallagher, T. Galloway, P. N. Butcher, T. M. Fromhold, B. G. Mulimani, and V. Karavolas, in *Proceedings of the 20th International Conference on the Physics of Semiconductors* edited by E. M. Anastassakis and J. D. Joannopoulos, pp. 853–856 (World Scientific, Singapore, 1990).
[8]J. P. Jay-Gerrin, Phys. Rev. B **12**, 1418 (1975).
[9]S. M. Puri, Phys. Rev. **139A**, 995 (1965).
[10]M. Lax, *Symmetry Principles in Solid State and Molecular Physics* (Wiley, New York, 1974).
[11]M. J. Smith and P. N. Butcher, J. Phys. Condens. Matter **1**, 4859 (1989).
[12]B. L. Gallagher, J. P. Oxley, T. Galloway, M. J. Smith, and P. N. Butcher, J. Phys. Condens. Matter **2**, 755 (1990).
[13]P. J. Price, Physica **134B**, 164 (1985).
[14]W. Cali, M. C. Marchetti, and M. Lax, Phys. Rev. B **34**, 8573 (1986).
[15]X. Zianni, P. N. Butcher, and I. Dharssi, J. Phys. Condens. Matter **4**, L77 (1992).
[16]T. Ando, A. B. Fowler, and F. Stern, Rev. Mod. Phys. **54**, 437 (1982).
[17]R. R. Gerhardts, Z. Phys. B **21**, 285 (1975).
[18]E. Gornik, R. Lassnig, G. Strasser, H. L. Stormer, A. C. Gossard, and W. Wiegmann, Phys. Rev. Lett. **54**, 1820 (1985).
[19]J. P. Eisenstein, H. L. Stormer, V. Narayanamarti, A. Y. Cho, A. C. Gossard, and C. W. Tu, Phys. Rev. Lett. **55**, 875 (1985).
[20]T. M. Fromhold, P. N. Butcher, G. Qin, B. G. Mulimani, J. P. Oxley, and B. L. Gallagher, Surf. Sci. **263**, 183 (1992).
[21]B. K. Ridley, *Quantum Processes in Semiconductors* (Clarendon, Oxford, 1988).
[22]Y. Murayama and T. Ando, Phys. Rev. B **35**, 2252 (1987).
[23]T. Ando and Y. Murayama, Phys. Soc. Jpn. **54**, 1519 (1985).
[24]I. S. Gradshteyn and I. M. Ryzhik, *Tables of Integrals, Series and Products* (Academic, New York, 1965).
[25]P. J. Price, Ann. Phys. (N.Y.) **133**, 217 (1981).